Supporting Information for "Gas seepage and pockmark formation from subsurface reservoirs: Insights from table-top experiment"

Inbar Vaknin,[1] Einat Aharonov*,[1] Ran Holtzman*,[2] and Oded Katz[3]

[1] *Institute of Earth Sciences, The Hebrew University of Jerusalem, Jerusalem, Israel*
[2] *Coventry University, Centre for Fluid and Complex Systems, Coventry, United Kingdom*
[3] *Geological Survey of Israel, Jerusalem, Israel**

Contents of this file

1. Text S1 to S3
2. Figures S1 to S2
3. Table S1

Additional Supporting Information (Files uploaded separately)

1. Captions for Movies S1 to S5

* einatah@mail.huji.ac.il; ran.holtzman@coventry.ac.uk

Introduction

Enclosed below as Supporting Information are analysis of gas pressure variation along the first part of two selected experiments (Text S1): Experiment #2D (plastic deformation mode that results in a Type-1 PM) and #1A (doming deformation mode that results in a Type-2 PM). Text S1 also includes data (Fig. S1) of gas pressure variations measured during the experiments with comparison to observed deformation events. Text 2 provides the dependency of the bubble radius and the clay (seal) thickness from the experiments (Fig. S2), which agrees with our theoretical prediction (Eq. 11 in main text). A detailed explanation of the choice of parameter values done for the theoretical calculation along the manuscript is given in Text 3 below. Five videos of selected experiments showing all modes of deformation described in the manuscript (doming, brittle, plastic) are also enclosed (Movies S1–S5).

Text S1. Analysis of gas pressure

In general, pressure buildup and drop cycles during the PMs formation (measured at the gas inlet syringe) follow the observed gas induced sill deformation and gas seepage events, respectively. Gas seepage requires a critical pressure value to keep the seepage conduit open, causing pressure to cycle. In the following, the pattern of pressure buildup and drop during two individual experiments (#2D: plastic deformation; #1A: doming) are described in comparison to their cyclic deformation and gas seepage events.

In the plastic deformation mode (Fig. S1a), gas pressure typically builds up until it reaches the capillary threshold of the sand. At that point, gas invades the sand layer causing a sudden drop in pressure due to the gas volume expansion. Since the capillary threshold of the sand is substantially higher than the pressure required for the plastic yielding of the clay, the first peak in Fig. S1a occurs well before breaching of the clay layer. After this peak, signifying gas invasion into the reservoir, pressure starts dropping. The pressure decrease continues while the clay layer is breached (yellow diamond marked II in Fig. S1a), which also corresponds to stage II in Fig. 3 (experiment #2D), and as gas seeps and transverses the clay layer (yellow diamonds marked III – V in Fig. S1a, and stage III–V in Fig. 3). At that point (∼230 seconds) the first seepage event is finished, and the gas conduit closes. With time, pressure recovers. Once the pressure exceeds the critical threshold required to reopen the pathway through the clay, another seep event occurs and the pressure drops again to its minimum value (∼600 seconds in Fig. S1a). From here on, repeated minor pressure build-ups and drops are recorded as a result of seepage events through a quasi-open pathway through the clay (e.g. yellow diamond marked VI in Fig. S1a, and snapshot VI for experiment #2D in Fig. 3).

The pressure variations in the doming deformation mode (Fig. S1b) typically evolve quite differently than the one describes above for the plastic mode. Initially, like in the plastic case, pressure builds up to the sand capillary threshold, after which it starts to drop. Pressure drop continues through doming initiation (yellow diamond marked II in Fig. S1b), which also corresponds to snapshot II in Fig. 3 (Experiment #1A) and the dome final expansion where the drop ceased (Pm1 in Fig. S1b). Then, pressure starts to build up again, and when it reaches a new critical value (Pc1 in Fig. S1b) the dome inflates abruptly (apparently due to reopening of the gas pathway), causing a pressure drop (to Pm2). Further expansion of the dome following pressure buildup (stage III) causes it to crack until it is breached (stage IV). Gas escapes through the breach (stage V) causing the pressure to drop again. Gas seepage requires a critical pressure value to keep the conduit between the clay blocks open, causing pressure to cycle, i.e. to increase when the conduit collapses and to decrease when it is reopened (similar to diking systems, e.g. Kelemen and Aharonov (1998)).

We note that during the experiments the pump heats up periodically (by 0.2^oC), and high-temperature peaks are minutes apart. At the max temperature, the injection rate decreases and results in short-duration events exhibiting a lower pressurization rate (Fig. S1).

Text S2. Analyzing bubble radius as function of clay (seal) thickness

Theoretically, we predict that bubble size increases with seal thickness (Eq. 11 in main text). Fig. S2 shows measured experimental results that verifies this dependency.

Text S3. Choice of parameter values

A complete list of parameters used in this paper and the choice of values (when applicable) is provided in Table S1. Densities of clay and water are $\rho_c = 1500$ and $\rho_w = 1000$ kg/m^3. In clay, the undrained friction angle, ϕ, is 20 - 45^o, following Ouyang and Mayne (2018). We use the lower value of $\phi = 20^o$ due to the very high water content and short settling time. In nature most soils are over-consolidated to some degree (Wood, 1991), $OCR > 1$. Here, as we used clay that settled in water under its own weight (lower normal stress than in nature), we expect the clay to be under- or normally-consolidated, $OCR \leq 1$. Thus, we use values of OCR=1 and OCR=0.5 for the experiments with $t_s = 6$ and 3 weeks, respectively. We use typical value of the exponent, $\gamma = 0.8$, following Sun and Santamarina (2019). Using the above parameter values, and the range of clay layer thickness tested here, $h_c = 0.007$ - 0.1m, Eq. 9 predicts c_u ranges of 8.5 - 85 and 4.9 - 49 Pa for t_s of 6 and 3 weeks, respectively.

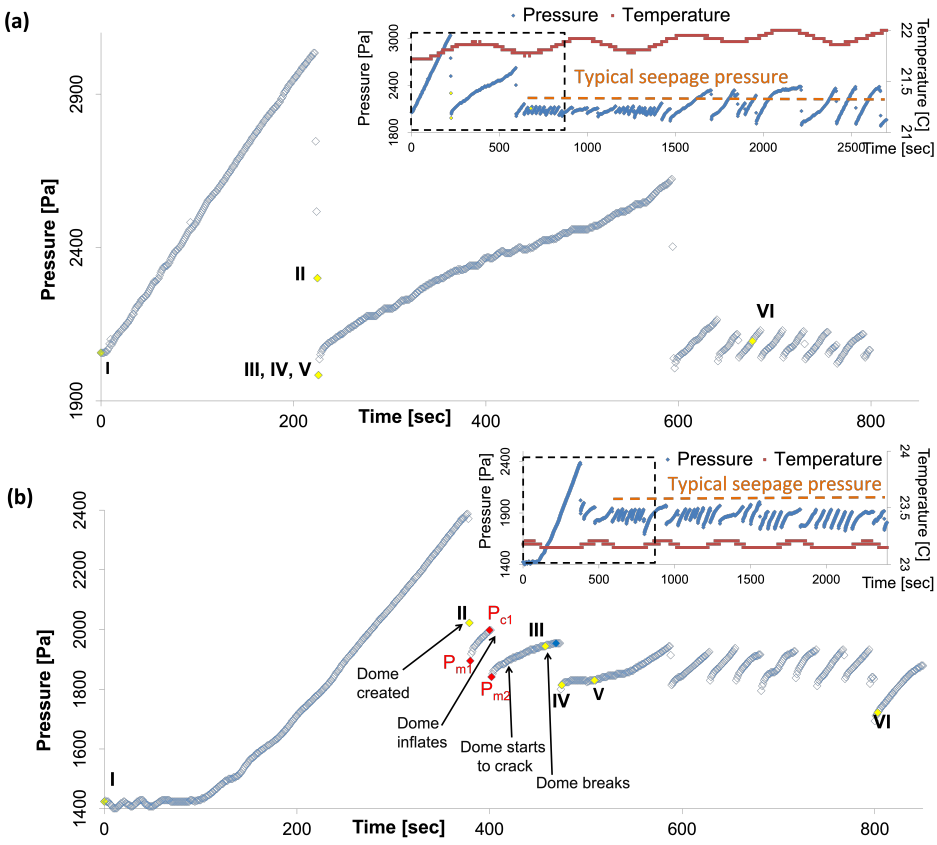

FIG. S1. Pressure variation (measured at the syringe pump outlet) along the first part of two selected experiments. (a) Experiment #2D (h_c = 3.8 cm): seal breaching by liquefaction around ascending gas bubble and development of Type-1 pockmark (see Table 1 in main text for more detail about the experimental setting). Yellow diamonds numbered I - VI are points presented by the snapshots in Fig. 3 in main text. Inset shows pressure and temperature variation along the entire experiment (dashed frame shows the time slot presented in details). Post breaching cyclic seepage pressure is marked by the orange dashed line; (b) Experiment #1A (h_c = 0.7 cm): Doming and breaching by fracturing of the dome and development of Type-2 pockmark. Yellow diamonds numbered I - VI are points presented by the snapshots in Figure 3. Inset shows pressure and temperature variation along the entire experiment (dashed frame shows the time slot presented in details). Post breaching cyclic seepage pressure is marked by the orange dashed line.

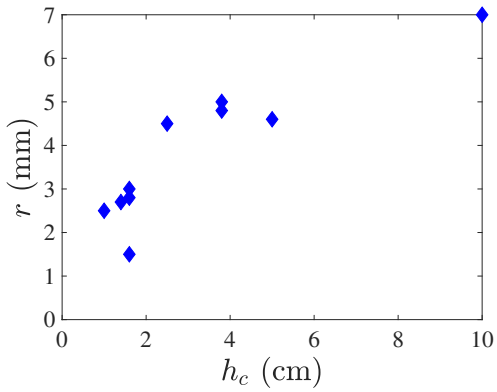

FIG. S2. Bubble radius r as a function of clay (seal) thickness h_c in experiments where the clay deformed plastically.

TABLE S1. Parameters used in the experiments and the analyses. See Text 3 for details of selection of values.

Symbol	Name	Values	Units
N	number of seepage events	0–25	-
h_c	clay layer thickness	0.007–1000	m
t_s	duration of clay settlement	3 or 6	weeks
D	pockmark depth	NA†	-
L	pockmark width	NA†	-
P_g	Gas pressure	NA†	-
P_w	Water pressure	NA†	-
ΔP	Gas overpressure	NA†	-
h_g	Gas pocket height	NA†	-
ρ_w	Water density	1000	kg/m^3
ρ_g	Gas density	1	kg/m^3
ρ_g	Clay density	1500 (experiments) 1890 (field)	kg/m^3
g	Gravitational acceleration	9.81	m/s^2
σ'_v	Effective stress (bottom of clay layer)	NA†	-
ΔP_{cavity}	Critical pressure to form a cavity	NA†	-
σ'_3	Effective stress (minor principal direction)	NA†	-
E	Young's modulus (of clay)	Eq. S1	Pa
ν	Poisson ratio (of clay)	0.3 [a]	-
c_u	Undrained shear strength (of clay)	Eq. 5 (main text)	Pa
ϕ	Undrained friction angle (of clay)	20	degrees
OCR	Overconsolidation ratio	0.5–1	-
r	Gas bubble radius	NA†	-
γ	Exponent relating strength and OCR	0.8 [b]	-
F_d	Drag force	NA†	-
F_b	buoyancy force	NA†	-
k	Empirical coefficient (for critical bubble radius)	NA†	-
ΔP_{dome}	Fracturing pressure (for dome)	NA†	-
ΔP_{plug}	Critical faulting pressure (for forming a plug)	NA†	-
T_0	Tensional strength (of clay)	5000-6000	Pa
a	Dome length	NA	
W	experimental cell width	15 or 50	cm
l	Plug length	1	cm
d	Spacing between cell walls (=plug thickness)	0.3	cm
F_{frac}	Faulting force	NA†	-
F_{slid}	Sliding force	NA†	-
n	Empirical factor (shear contribution to fracturing)	$\sim$1.25 [c]	-
ϕ_w	Clay-wall friction angle	7	-

† Non-applicable (e.g. parameter value continuously changes).
[a] Marchi *et al.* (2014).
[b] Sun and Santamarina (2019).
[c] Atkinson *et al.* (1994).

In computing the sliding force (Eq. 4 in main text) we use the following parameter values: $n = 1.25$ (Atkinson 2017) $\mu_c = \tan(\phi)$ and plug width of $l \approx 1$ cm (from analysis of our experimental images). For lack of measured values of the friction coefficient of udrained Kaolinite against Plexiglas, we consider a value of $\phi_w = 7^o$ (Xu *et al.* 2018).

The spacing between the plexigalss walls is $d = 3$ mm. We use $\nu = 0.3$ for the Poisson ratio of clay (Marchi *et al.* 2014). We note that the Young's modulus E increases with settlement time, t_s, due to chemo-mechanical consolidation and time-dependent changes in clay outer layer electric charge effecting bonding (Marcuson and Wahls 1972, Mukabi and Hossain 2011). To examine this effect of varying E, we used two settling times t_s, 3 and 6 weeks. Multiple studies have found that E also grows monotonically with effective stress (Ishihara 1996, Chapman and Godin 2001, Snieder and Beukel 2004). As we did not measure experimentally E, we adopt the following functional dependence of E as a function of the OCR and the effective stress (Athanasopoulos 1993):

$$E = A{\sigma'_v}^{0.58} OCR^{0.42} \tag{S1}$$

where A=20000 for the experiments and 2000 for the field. This provides E values ranging between $130kPa$ to $27MPa$ for h_c ranging from 0.01-1000 m. This approximately agrees with the range provided by (Koch *et al.* 2015).

For the field calculations we use a higher clay density of $1890kg/m^3$. For dome dimensions we use $a = 5h_c$, $w_{max} = 0.03a$ (Koch *et al.* 2015), noting the uncertainty due to the large variability in these values.

Movie captions

Movie S1. Video of experiment #1A showing doming initial deformation mode and consequent Type-2 pockmark formation as seepage continues. Lower dark layer is the sand reservoir, middle gray layer is the clay seal ($h_c = 0.7$ cm), upper dark layer is the water. For more details of the experimental conditions see Table 1 in main text.

Movie S2. Video of experiment #5E (wide experimental box) showing doming initial deformation mode and consequent Type-2 pockmark formation as seepage continues. The final pockmark is a result of integration of two seepage sites. Lower dark layer is the sand reservoir, middle gray layer is the clay seal ($h_c = 1.7$ cm), upper dark layer is the water. For more details of the experimental conditions see Table 1 in main text.

Movie S3. Video of experiment #5D showing brittle (faults bounded plug) initial deformation mode and consequent Type-1 pockmark formation as seepage continues. The final pockmark is asymmetric a result of integration of two seepage sites. Lower dark layer is the sand reservoir, middle gray layer is the clay seal ($h_c = 2.2$ cm), upper dark layer is the water. For more details of the experimental conditions see Table 1 in main text.

Movie S4. Video of experiment #2D showing plastic (bubble ascending) initial deformation mode and consequent Type-1 pockmark formation as seepage continues through damage chimney. Lower dark layer is the sand reservoir, middle gray layer is the clay seal ($h_c = 3.8$ cm), upper dark layer is the water. For more details of the experimental conditions see Table 1 in main text.

Movie S5. Video of experiment #4E (wide experimental box) showing plastic (bubble ascending) initial deformation mode and consequent Type-1 pockmark formation as seepage continues through damage chimney. Lower dark layer is the sand reservoir, middle gray layer is the clay seal ($h_c = 10.0$ cm), upper dark layer is the water. For more details of the experimental conditions see Table 1 in main text.

SUPPLEMENTARY REFERENCES

P. B. Kelemen and E. Aharonov, Periodic formation of magma fractures and generation of layered gabbros in the lower crust beneath oceanic spreading ridges, Geophysical monograph **106**, 267 (1998).

Z. Ouyang and P. W. Mayne, Effective friction angle of clays and silts from piezocone penetration tests, Canadian Geotechnical Journal **55**, 1230 (2018).

Z. Sun and J. C. Santamarina, Grain-displacive gas migration in fine-grained sediments, Journal of Geophysical Research: Solid Earth **124**, 2274 (2019).

J. Atkinson, *The mechanics of soils and foundations* (CRC press, 2017).

C. Xu, X. Wang, X. Lu, F. Dai, and S. Jiao, Experimental study of residual strength and the index of shear strength characteristics of clay soil, Engineering Geology **233**, 183 (2018).

M. Marchi, G. Gottardi, and K. Soga, Fracturing pressure in clay, Journal of Geotechnical and Geoenvironmental Engineering **140**, 04013008 (2014).

W. F. Marcuson and H. E. Wahls, Time effects on dynamic shear modulus of clays, Journal of the Soil Mechanics and Foundations Division **98**, 1359 (1972).

J. N. Mukabi and Z. Hossain, Characterization and modeling of various aspects of pre-failure deformation of clayey geomaterials–applications in modelling, in *Proceedings. 1st International Conference. on Geotechnique, Environment & construction Materials, GEOMAT, Mie, Japan* (2011).

K. Ishihara, *Soil behaviour in earthquake geotechnics* (Clarendon press Oxford, 1996).

D. M. Chapman and O. A. Godin, Dispersion of interface waves in sediments with power-law shear speed profiles. ii. experimental observations and seismo-acoustic inversions, The Journal of the Acoustical Society of America **110**, 1908 (2001).

R. Snieder and A. v. d. Beukel, The liquefaction cycle and the role of drainage in liquefaction, Granular Matter **6**, 1 (2004).

G. A. Athanasopoulos, Effects of ageing and overconsolidation on the elastic stiffness of a remoulded clay, Geotechnical & Geological Engineering **11**, 51 (1993).

S. Koch, C. Berndt, J. Bialas, M. Haeckel, G. Crutchley, C. Papenberg, D. Klaeschen, and J. Greinert, Gas-controlled seafloor doming, Geology **43**, 571 (2015).

J. Atkinson, J. Charles, and H. Mhach, Undrained hydraulic fracture in cavity expansion tests, in *International conference on soil mechanics and foundation engineering* (1994) pp. 1009–1012.